Earth and Planetary Science Letters 413 (2015) 167–175

Contents lists available at ScienceDirect

Earth and Planetary Science Letters

www.elsevier.com/locate/epsl

Complex seismic anisotropy beneath western Tibet and its geodynamic implications

Jing Wu [a,b], Zhongjie Zhang [a], Fansheng Kong [b], Bin B. Yang [b], Youqiang Yu [b], Kelly H. Liu [b], Stephen S. Gao [b,*]

[a] State Key Laboratory of Lithospheric Evolution, Institute of Geology and Geophysics, Chinese Academy of Sciences, Beijing, China
[b] Geology and Geophysics Program, Missouri University of Science and Technology, Rolla, MO 65409, USA

ARTICLE INFO

Article history:
Received 8 October 2014
Received in revised form 31 December 2014
Accepted 2 January 2015
Available online 21 January 2015
Editor: A. Yin

Keywords:
seismic anisotropy
crustal flow
Tibetan Plateau

ABSTRACT

Shear wave splitting parameters obtained along a linear array of 23 stations deployed in western Tibet during a two-year period from 2011 to 2013 demonstrate strong and systematic azimuthal variations with a 90-degree periodicity, suggesting the existence of double-layer anisotropy with a horizontal axis of symmetry. The predominant fast orientations are mostly E–W for events from the east and southeast, and NE–SW or N–S for events from the northwestern quadrant. Under the assumption of a two-layer anisotropic structure, we grid-search for the two pairs of parameters that characterize the complex anisotropy. The resulting fast orientation for the lower layer is mostly N–S, which is consistent with the direction of mantle flow caused by the subduction of the Indian continent beneath Tibet. For the upper layer, the fast orientation is NE–SW, which is significantly different from the strike of dominant surface structures, and can be explained by lower crustal flow in western Tibet. This interpretation is supported by the NE–SW orientation and significant strength (with splitting times as large as 1.3 s) of crustal anisotropy revealed using the sinusoidal moveout of the P-to-S converted phases from the Moho. To our knowledge, this is the first time when upper layer anisotropy revealed from SWS analysis is reliably constrained in the crust using independently determined crustal anisotropy measured by the P-to-S converted phase from the Moho. The observations provide additional evidence for the existence of a subducted Indian slab that is undeformed and is decoupled from the significantly shortened crust, extending to the northern margin of the Qiangtang block.

1. Introduction

The Tibetan Plateau (Fig. 1) is generally considered as the result of continental collision between the Indian and Eurasian plates since ~70 Ma (Molnar and Tapponnier, 1975; Yin and Harrison, 2000). In spite of numerous studies, the 3-D distribution of the subducted Indian mantle lithosphere and the mechanisms responsible for the uplifting of the Plateau remain enigmatic (Yin and Harrison, 2000; Klemperer, 2006). While some studies advocate thickening of both the crustal and mantle parts of the lithosphere (Flesch et al., 2005), some others hypothesize that the uplift is mostly the result of crustal thickening associated with lower (and/or middle) crustal flow (Zhao and Morgan, 1987; Nelson et al., 1996; Klemperer, 2006; Royden et al., 2008; Zhao et al., 2013; Liu et al., 2014). The second hypothesis implies that the Indian mantle lithosphere is decoupled from the crust and may have experienced limited amount of shortening (Tapponnier et al., 2001).

Another debated issue is the 3-D distribution of the subducted Indian plate. Beneath central Tibet, along a N–S oriented profile (approx. 90°E), Tilmann et al. (2003) reveal a seismically fast region extending from 100 to 400 km depth beneath the northern Lhasa block, and interpret it as the near-vertically subducting Indian mantle lithosphere. Similarly, many shearwave splitting (SWS) and seismic tomography studies recognize sudden changes in mantle velocities and anisotropic properties beneath the Lhasa Block, probably associated with the northern extreme of the Indian mantle lithosphere, or a sharp transition from flat to near-vertical subduction (Huang et al., 2000; Li et al., 2008; Chen et al., 2010; Kind and Yuan, 2010). This transition is characterized by a boundary separating two areas with contrasting splitting times in eastern Tibet (Fig. 1). Large (1.5 s) splitting times with E–W or NE–SW station-averaged fast polarization orientations are frequently found north of this boundary, while small or zero (null mea-

* Corresponding author.
E-mail address: sgao@mst.edu (S.S. Gao).

http://dx.doi.org/10.1016/j.epsl.2015.01.002
0012-821X/

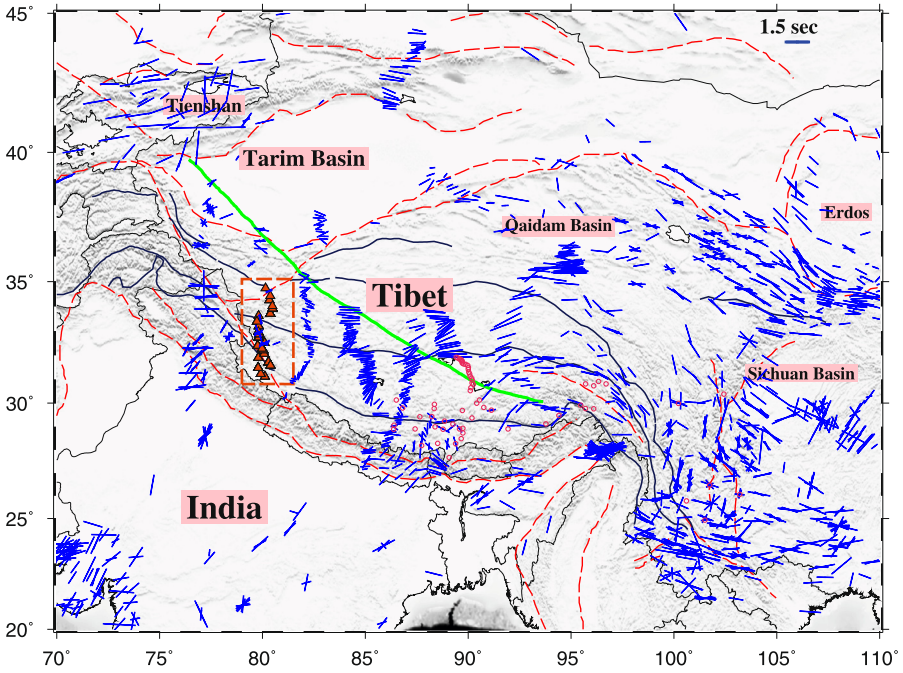

Fig. 1. Topographic map of the Tibetan Plateau showing major tectonic provinces and previous shear wave splitting measurements (Levin et al., 2008; Oreshin et al., 2008; Zhao et al., 2010. The rest are from http://splitting.gm.univ-montp2.fr/DB/public/searchdatabase.html). Circles show null measurements. Major faults are plotted as dashed brown lines, and suture zones are shown as black curves (Taylor and Yin, 2009). The thick green line shows the location of the Indian plate at the depth of 200 km (Kind and Yuan, 2010). The study area is outlined by the dashed rectangle, and the stations used in the study are shown as red triangles. (For interpretation of the references to color in this figure legend, the reader is referred to the web version of this article.)

surements) splitting times are found in the south (Fig. 1). Some other seismic tomography studies (e.g., Zhou and Murphy, 2005; Zheng et al., 2007; Zhao et al., 2014b), however, advocate the presence of Indian lithosphere beneath the entire Tibetan Plateau.

Numerous SWS studies (e.g., Silver and Chan, 1991; Silver, 1996; Savage, 1999) suggest that SWS analysis is a robust tool for characterizing mantle deformation and structure. Splitting of P-to-S converted phases (XKS, including SKS, SKKS, and PKS) from the core–mantle boundary provides the best lateral resolution of seismic anisotropy beneath the receiver side due to the steep angle of incidence of the XKS arrivals. The two splitting parameters, polarization orientation of the fast wave (ϕ or fast orientation) and the splitting time between the fast and slow waves (δt), quantify the orientation and magnitude of seismic anisotropy. Many previous investigations indicate that seismic anisotropy in the upper crust is mostly related to stress-aligned fluid-saturated cracks (Crampin, 1981), anisotropy in the lower continental crust is mostly the result of lattice preferred orientation (LPO) of anisotropic minerals in response to plastic flow (Aspiroz et al., 2007; Tatham et al., 2008), and that in the mantle is the consequence of strain-induced LPO of intrinsically anisotropic mantle minerals, principally olivine (Zhang and Karato, 1995).

Due to the essentiality of SWS in characterizing crustal and mantle deformation, a large number of SWS studies have been conducted in Tibet (Fig. 1) (e.g., McNamara et al., 1994; Sandvol et al., 1997; Huang et al., 2000; Gao and Liu, 2009; Chen et al., 2010; Zhao et al., 2010; Zhao et al., 2014a). In western Tibet, which is the focus of this study, the majority of the fast orientations from previous studies are E–W or NE–SW (Oreshin et al., 2008; Levin et al., 2008; Zhao et al., 2010), with rapid lateral variations (Fig. 1). A total of 52 measurements from SKS (Oreshin et al., 2008) and 85 measurements from SKS and PKS (Levin et al., 2008) have been obtained in the vicinity of our study area (Fig. 1). Interestingly, the sudden northward increase of δt observed in central and eastern Tibet is not seen in western Tibet.

For most of the SWS studies in Tibet, the limited number of event-specific measurements and inadequate azimuthal coverage of the events prevented investigations of complex anisotropy such as that recognized at station LSA (29.70°N, 91.15°E) by Gao and Liu (2009). Such complex anisotropy is characterized by systematic back azimuthal variations of the splitting parameters. This study takes the advantage of a recently recorded XKS data set to investigate crustal and mantle anisotropy beneath western Tibet, for the purpose of characterizing crustal and mantle flow and deformation, as well as providing independent constraints on the geometry of the subducted Indian mantle lithosphere.

2. Data and methods

The broadband seismic data used in the study were recorded by 23 portable seismic stations located along an approximately N–S profile in the area of 31–35°N and 80–81°E (Fig. 2). The stations were installed and operated by the Institute of Geology and Geophysics of the Chinese Academy of Sciences during the time period of 11/2011–11/2013 (Zhang et al., 2014). The profile, which is named as TW-80, traversed the Himalayan, Lhasa, and Qiangtang Blocks, which are separated by lithospheric suture zones (Taylor and Yin, 2009). Each of the stations was equipped with a Guralp CMG-3ESP seismometer and a Reftek-72A digitizer.

2.1. XKS splitting

In this study, seismograms from earthquakes of magnitude 5.6 (which is reduced to 5.5 for events with a focus deeper than 100 km) or greater were extracted for SWS analysis, using the procedure described in Liu and Gao (2013), which was based on the minimization of transverse energy approach of Silver and Chan (1991). The epicentral distance range is 84–180°, 120–180°, and 90–180° for SKS, PKS, and SKKS, respectively. The seismograms were band-pass filtered with corner frequencies of 0.04 and 0.5 Hz

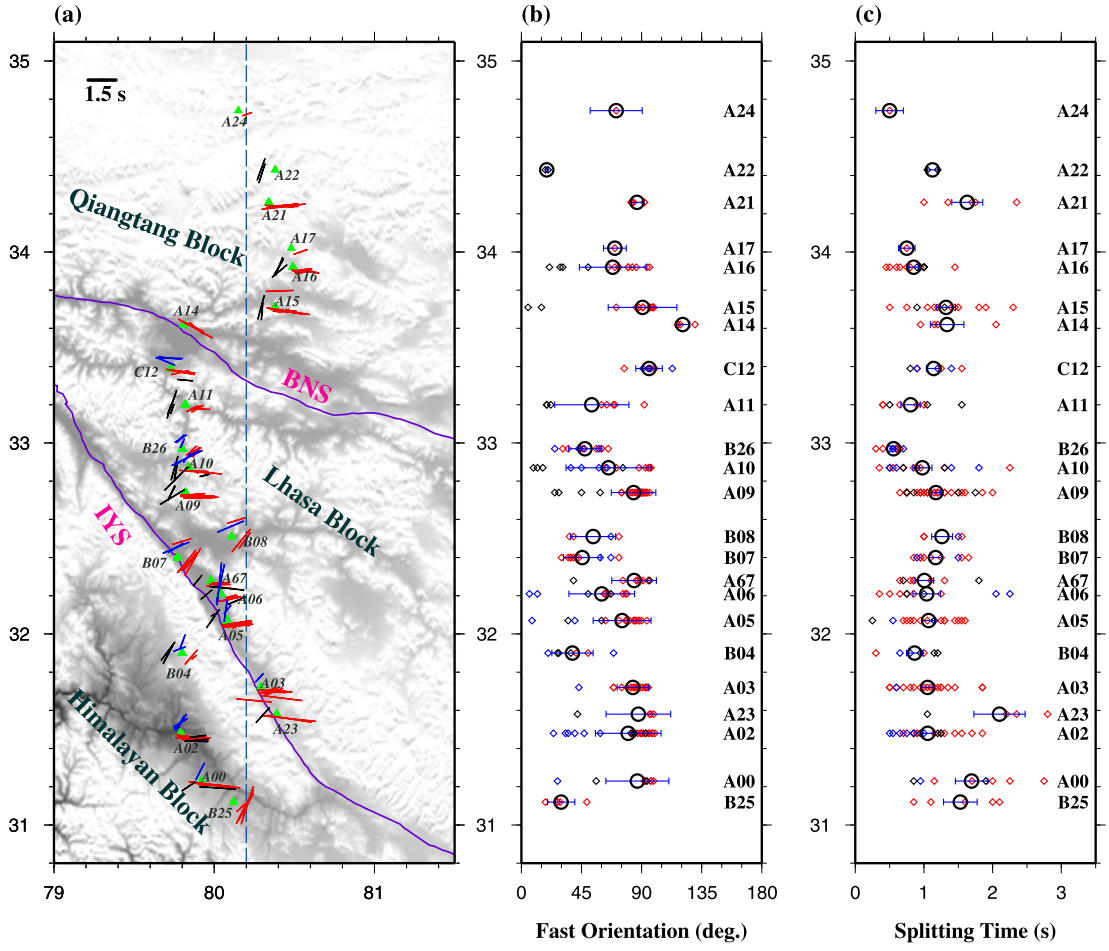

Fig. 2. Resulting shear wave splitting measurements. (a) Measurements plotted above ray-piercing points at 50 km deep on a topographic map. Purple lines are sutures (BNS: Bangong Nujiang suture; IYS: Indus Yalu suture). Measurements from SKS, SKKS and PKS are shown in red, black, and blue respectively. (b) Fast orientations (small diamonds) plotted at the latitude of the recording stations. The large circles show the average fast orientation observed at each of the stations. (c) Same as (b) but for splitting times. Note that the first letter in the station name indicates the group that the station belongs to. (For interpretation of the references to color in this figure legend, the reader is referred to the web version of this article.)

which is the main frequency band of the XKS phases. Those with a signal to noise ratio (SNR) lower than 4.0 on the original radial component were not used for SWS analysis (see Liu and Gao, 2013 for the specific definition of the SNR).

SWS measurements were then conducted on the selected seismograms, and ranking of resulting measurements was performed using a combination of the SNR values on the original radial, original transverse, and corrected transverse components (Liu et al., 2008). Manual checking was applied to each of the measurements. During the manual checking stage, the start and end times of the XKS window, the band-pass filtering parameters, and results of automatic ranking were visually verified, and adjusted if necessary to ensure reliable results (Liu, 2009).

2.2. Crustal anisotropy

In addition to XKS splitting, in this study we also utilize systematic azimuthal variations of the arrival time of the P-to-S converted phase from the Moho, Pms, for the purpose of quantifying crustal contributions to the observed XKS splitting. Data from magnitude ≥4.0 earthquakes in the epicentral distance of 30–180° are filtered in the frequency band of 0.08–0.8 Hz and subsequently used to compute radial receiver functions (RFs) using the procedure of Ammon (1991). As described in a number of previous studies (Liu and Niu, 2012; Rumpker et al., 2014), when Pms travels through a simple weakly anisotropic layer, the apparent moveout can be expressed as

$$t_{Pms} = t_0 - \frac{\delta t_c}{2}\cos\left[2(\alpha - \phi_c)\right] \quad (1)$$

where t_0 is the reference time which is the arrival time of Pms when the crust is isotropic, δt_c is the amplitude of the arrival time moveout caused by crustal anisotropy and is also the splitting time associated with crustal anisotropy, α is the back-azimuth of the RF, and ϕ_c is the crustal fast polarization orientation.

We grid-search for the optimal combination of t_0, ϕ_c, and δt_c that gives the maximum stacking amplitude, by stacking the RFs. The searching range for ϕ_c is 0–180° with a step of 1°. Because the study area probably possesses the thickest crust and largest crustal anisotropy in the world due to the significant shortening and possible lower crustal flow, the searching range for δt_c is set as 0.0–1.5 s with a step of 0.05 s, and that for t_0 is 5–12 s with a step of 0.1 s.

A couple of steps are taken to increase the reliability of the resulting crustal splitting parameters. First, to minimize the effects of the variations of Pms arrival times associated with varying epicentral distances, the arrival times are corrected to a uniform epicentral distance of 60°. Second, RFs within 10°azimuthal bins are averaged before the stacking for the purpose of avoiding dominance by RFs from a single or a limited number of BAZ bands.

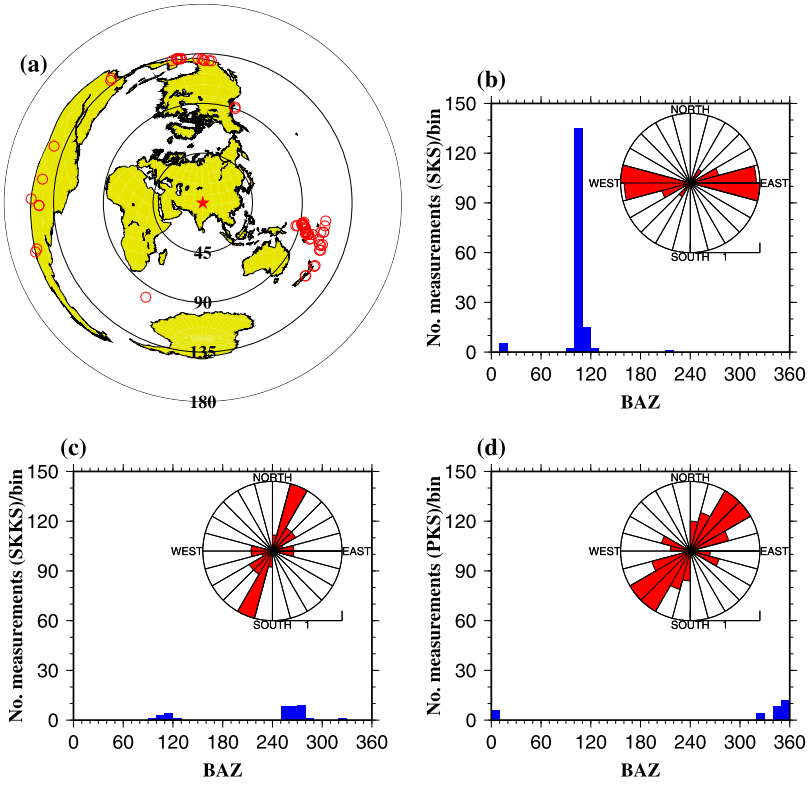

Fig. 3. (a) An azimuthal equidistant project map of the world centered at the study area, showing the distribution of earthquakes used in the study. (b) A histogram showing the back azimuths of the SKS measurements. The inset is a rose diagram of fast orientations resulted from SKS. (c) Same as (b), but for SKKS measurements. (d) Same as (b), but for PKS measurements.

3. Results

3.1. Spatial and azimuthal variations of XKS splitting parameters

A total of 224 pairs of well-defined (quality A and B based on the ranking criteria of Liu et al., 2008) XKS splitting parameters were obtained, including 28 from PKS, 36 from SKKS, and 160 from SKS (Fig. 2). Four of the stations with a total of 41 measurements are on the Himalayan, 13 stations with 148 measurements are on the Lhasa, and 6 stations with 35 measurements are on the Qiangtang blocks. The average splitting time over all the measurements is 1.10 ± 0.48 s, and that for the Himalayan, Lhasa, and Qiangtang blocks is 1.20 ± 0.53, 1.07 ± 0.46, and 1.14 ± 0.49 s, respectively. Due to the location of the study area relative to the current global earthquake distribution (Fig. 3a), the vast majority of the SKS measurements have a BAZ in a narrow band centered at 110° (Fig. 3b), and all the PKS events were approximately from the north (Fig. 3d). About 1/3 of the SKKS measurements have a BAZ of about 110°, and the rest have a westerly BAZ (Fig. 3c).

The 23 stations can be divided into 3 groups based on the characteristics of azimuthal variations of the splitting parameters. Group A, which includes 17 of the 23 stations (Fig. 2b), is characterized by systematic azimuthal dependence of the splitting parameters (Fig. 4) with a 90°periodicity. For stations in this group, events from the SE result in approximately E–W fast orientations, while events from the NW quadrant lead to NE–SW fast orientation (see Fig. 5 for examples). In the next section, these stations are used for grid-searching for the two sets of SWS parameters that characterizing the two layers. Group B includes five stations (Fig. 4). They are characterized by approximately NE–SW fast orientations, with less significant azimuthal variations than Group A. For two of the stations (B07 and B08) in this group, events from the SE result in more northerly fast orientations than those from the north (Fig. 2), while other stations (B04 and B26) show azimuthally independent fast orientations or insufficient azimuthal coverage (B25, Fig. 2). Group C has only one station (C12). Measurements at this station are not azimuthally dependent, and the fast orientations are mostly E–W. The three SKS and one SKKS measurements obtained at this station are E–W, similar to those observed at Group A stations. This station is not included in Group A because the 3 PKS measurements are E–W, not NE–SW (Fig. 4). Given the limited number of measurements, results from this station are not discussed below.

3.2. Crustal anisotropy from Pms

The clear systematic azimuthal variations of the splitting parameters with a 90° periodicity observed at the majority of the stations (Fig. 4) suggest the existence of multiple layers of anisotropy with a horizontal axis of symmetry (Silver and Savage, 1994). To explore the possibility that the top layer resides in the crust, we next attempt to quantify crustal anisotropy beneath each of the stations by modeling azimuthal variations of the arrival time of P-to-S conversions from the Moho, using the procedure described in Section 2.2.

In order for the procedure to give reliable results, a number of conditions must be met. The first is that crustal anisotropy beneath the station can be characterized by a single layer of anisotropy with a horizontal axis of symmetry (Rumpker et al., 2014). Second, there must be an adequate azimuthal coverage in order to obtain a reliable pair of crustal splitting parameters by fitting the azimuthal variation of the Pms arrival times. Such a coverage is dependent on the duration of recording, station performance, and the location of the station relative to the world's major seismic belts. Third, the Moho must be sufficiently sharp and smooth so that robust Pms arrivals can be generated. Previous crustal RF studies in Tibet

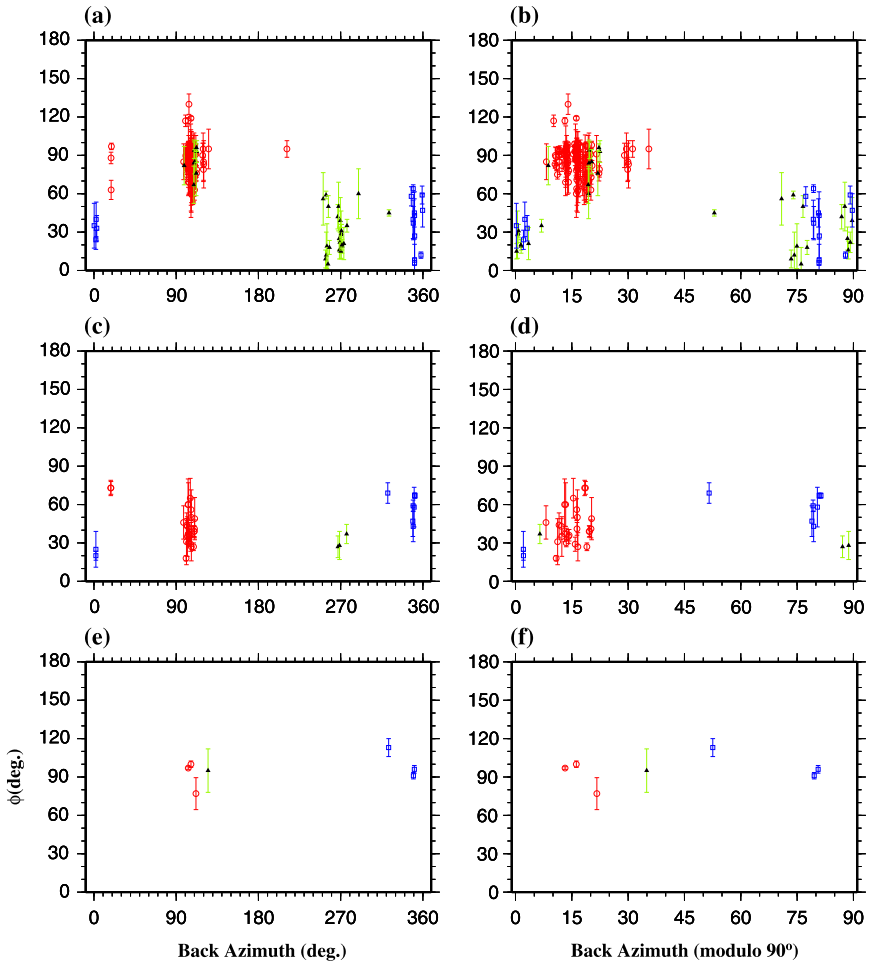

Fig. 4. Azimuthal variations of resulting fast orientations for group A (top panels), group B (middle), and group C (bottom) stations. The red circles, black triangles, and blue squares represent SKS, SKKS, and PKS phases, respectively. (For interpretation of the references to color in this figure legend, the reader is referred to the web version of this article.)

indicate that the Pms is complicated and weaker than typical continental areas, probably due to the thicker and abnormally heterogeneous crust (Ozacar and Zandt, 2004). Finally, crustal thickness and velocities in the vicinity of the station must be approximately uniform. Lateral variations of crustal properties can result in azimuthal dependence of Pms arrival times that are not associated with crustal anisotropy, leading to incorrect results.

After visual inspections of all the RFs recorded by each of the stations, only three of the 23 stations (B04, A05, and A09) satisfy the above conditions (Fig. 6). The resulting ϕ_c values range from 14–44°, and the δt_c values are between 0.45–1.30 s, and the average values are $33 \pm 16.5°$ and 0.83 ± 0.43 s. The crustal splitting times are significantly larger than most of those found by previous studies (McNamara and Owens, 1993; Chen et al., 2013), suggesting a thicker anisotropic layer and/or a larger degree of anisotropy beneath the study area relative to most other areas on the Earth. For a lower/middle crustal layer of 40 km thick, the observed splitting times require an anisotropy of 5–15%. This high degree of anisotropy has been reported in lower crustal schist (Okaya et al., 1995). Note that the first arrival of some of the RFs is delayed by a fraction of a second (Fig. 6), a phenomenon that is commonly attributed to the delay effects of near-surface loose sediments (Yeck et al., 2013). While this small delay time can lead to errors in the resulting crustal thickness (which is not the subject of this study), the non-systematic azimuthal variations of the delays suggest that they have negligible impact on the results quantifying crustal anisotropy (Rumpker et al., 2014).

4. Discussion

4.1. Characterization of two-layer anisotropy

The systematic azimuthal variations of the splitting parameters with a 90° periodicity for Group A and perhaps Group B stations (Fig. 7) indicate the existence of multiple-layers of anisotropy with horizontal axes of symmetry. Under the assumption of a two-layer model, which is the simplest form of multiple-layer anisotropy, we grid-search for the two pairs of parameters beneath Group A stations using the approach of Silver and Savage (1994). To reduce the well-known non-uniqueness of the grid-searching procedure (e.g., Gao and Liu, 2009), we use results of crustal anisotropy as *a priori* constraints by restraining the fast orientation of the top layer to the first quadrant (0–90°). The resulting splitting parameters that fit observations reasonably well are (5°, 1.2 s) for the lower layer, and (45°, 1.0 s) for the upper layer (Fig. 7). While some other combinations of the parameters can also fit the observations reasonably well, it is clear that a model with a nearly N–S fast orientation for the lower layer and a NE–SW fast orientation for the upper layer can satisfactorily explain the azimuthal variations.

Observations at Group B stations lack both significant azimuthal variations and sufficient azimuthal coverage, preventing a formal grid-search. However, the observations can be explained by a two layer model with similar individual layer splitting parameters as that for Group A station, except that the splitting time for the up-

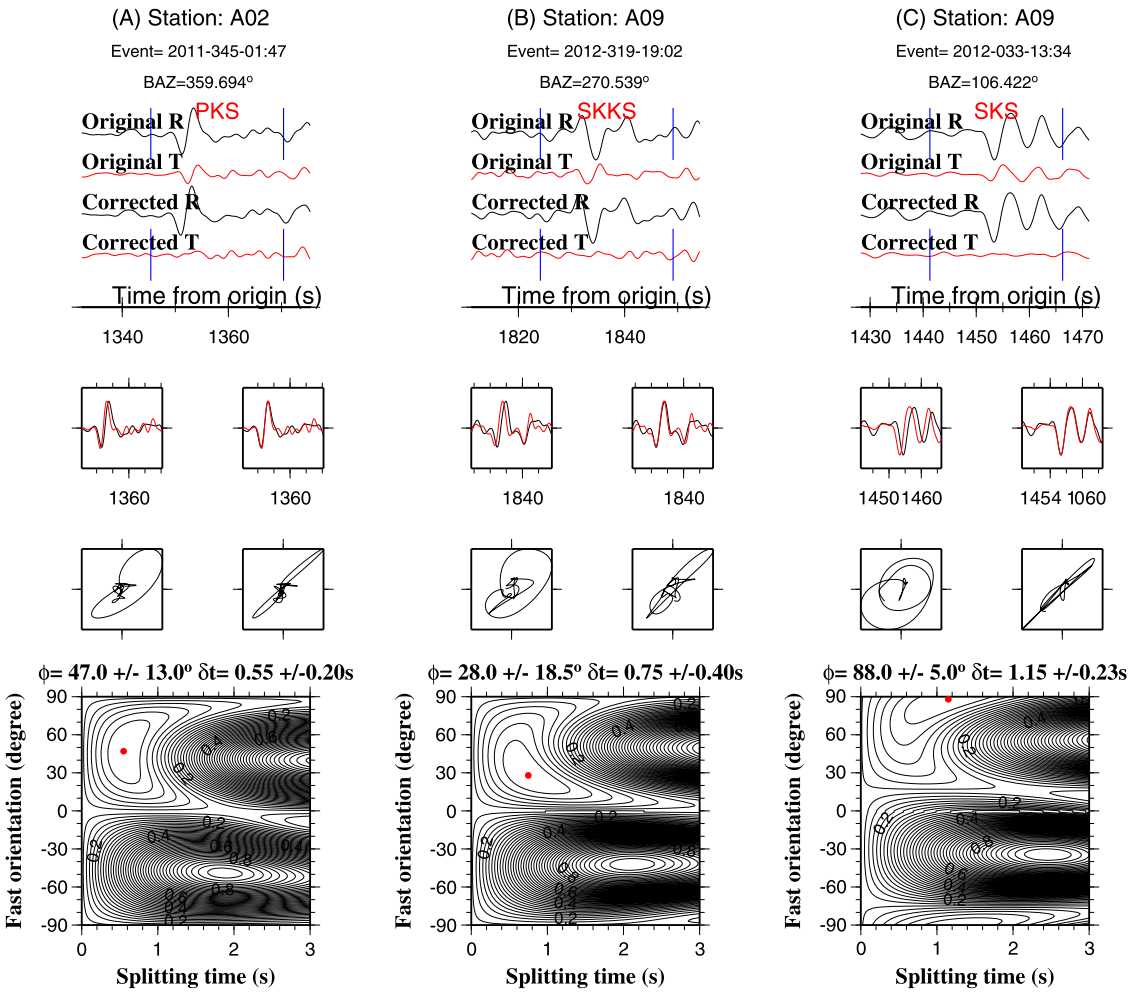

Fig. 5. (From top to bottom) Original and corrected radial and transverse components, their particle motion patterns, and the contour of normalized energy on the corrected transverse component for three events recorded by two stations (see labels at the top for event and station names).

per layer needs to be reduced from 1.0 to about 0.6 s (Fig. 7). Note that attempts have been made to use data from individual stations or groups of nearby stations to search for the 2-layer parameters, using the same procedure that Gao and Liu (2009) applied to 15-years of data from a Global Seismographic Network (GSN) station, LSA, in eastern Tibet. Unfortunately, due to the short (2 yr) recording duration and less vigorous site selection and construction standards (relative to a GSN station) used for the portable TW-80 stations, reliable results cannot be obtained. While combining data from stations with similar azimuthal variations can improve the azimuthal coverage and thus the reliability of the resulting 2-layer parameters, the combination may lead to scatterness in the observed data (Fig. 4), due to variations in detailed anisotropic structure beneath the stations. Therefore, the resulting 2-layer parameters represent a regionally averaged rather than station-specific anisotropic structure.

4.2. Formation mechanisms of the observed anisotropy

The consistency between the upper layer splitting parameters and results from crustal anisotropy analysis suggests that the upper layer resides in the crust, probably due to plastic crustal flow which aligns anisotropic minerals such as amphibole (Aspiroz et al., 2007; Tatham et al., 2008). The NE–SW orientation of the observed anisotropy is consistent with that of middle-lower crustal flow (Fig. 2) suggested using seismic refraction and geodynamic modeling (Klemperer, 2006). The reduction of the splitting times revealed at Group B stations might be the result of local weakening of the crustal flow.

The resulting splitting parameters for the lower layer can be explained by a model involving simple shear between the partially coupled lithosphere and underlying asthenosphere. The dominant structures (mostly sutures) as well as the direction of maximum lithospheric extension in the study area are approximately SE–NW, which would lead to SE–NW fast orientations if lithospheric fabrics dominate. The fact that the fast orientation of the lower layer is nearly N–S suggests that the sub-crustal lithosphere has limited contribution to the observed anisotropy. In contrast, the fast orientation for the lower layer is consistent with most of the fast orientations observed on the Indian continent (Fig. 1), which has been moving towards the North since at least 100 Ma (Kent, 1989). Such a long term movement may produce preferred orientation of olivine in the lower lithosphere and the upper asthenosphere, leading to observable anisotropy. This mechanism has been used by Elsheikh et al. (2014) to explain dominantly N–S fast orientations observed in Arabia and northern Africa.

4.3. Geodynamic implications

The observations and the resulting two-layer model provide constraints on a number of controversial issues regarding Tibetan crustal and mantle deformation and dynamics. The first of such issues is whether the entire Tibetan lithosphere deforms coherently as a thin viscous layer (Molnar et al., 1993), or the shortening is

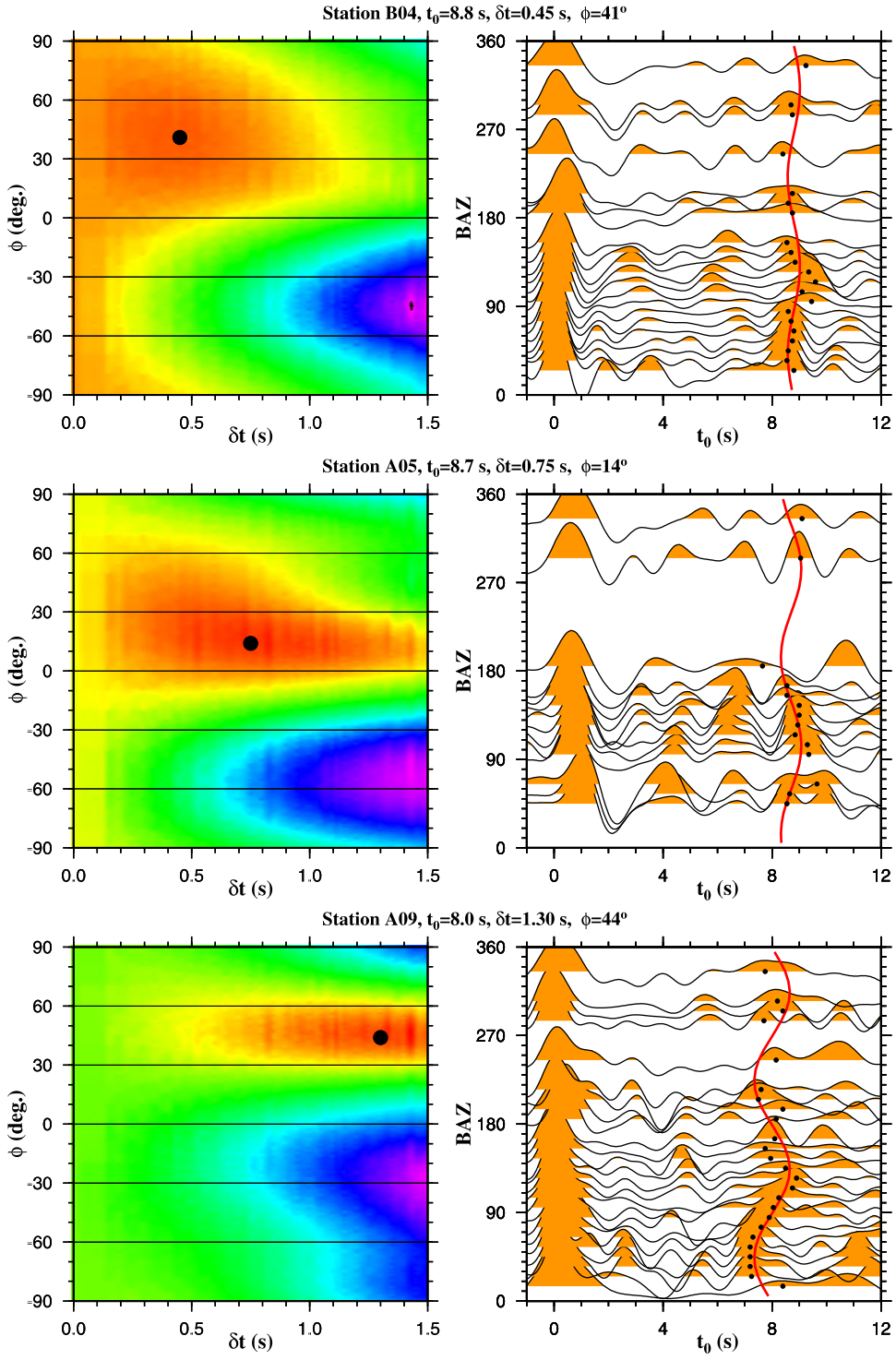

Fig. 6. Crustal anisotropy measurements estimated using data recorded by stations B04 (upper), A05 (middle), and A09 (lower). The image maps (left) show the stacking amplitudes calculated based on all candidate pairs of fast orientations and delay times. The radial receiver function traces are plotted against BAZ (right). The small black dots are the peak locations of the Pms conversions. The red curve represents the theoretical Pms moveout estimated by Eq. (1) using the optimal pair of splitting parameters (which are marked by the black dot on the left plots). (For interpretation of the references to color in this figure legend, the reader is referred to the web version of this article.)

only limited to the crust (Tapponnier et al., 2001). The former predicts a simple anisotropy with a SE–NW fast orientation which is at a large angle with the shortening direction (England and Molnar, 2005) and is not observed. Therefore, at least for the study area, results presented here are inconsistent with coherent lithospheric shortening.

The second issue is the existence and geometry of the subducted Indian plate. Mostly based on seismic tomography and receiver function studies, a number of models have been proposed, such as stacking of multiple slabs beneath the Himalayan and Lhasa blocks (Kumar et al., 2005; Li et al., 2008; Royden et al., 2008), and the existence of a nearly flat Indian slab beneath the entire Tibetan Plateau (Zhou and Murphy, 2005; Zheng et al., 2007; Zhao et al., 2014b). SWS measurements in central and eastern Tibet show a sharp transition from small splitting times to large ones (Fig. 1). In contrast, there are no significant changes in the charac-

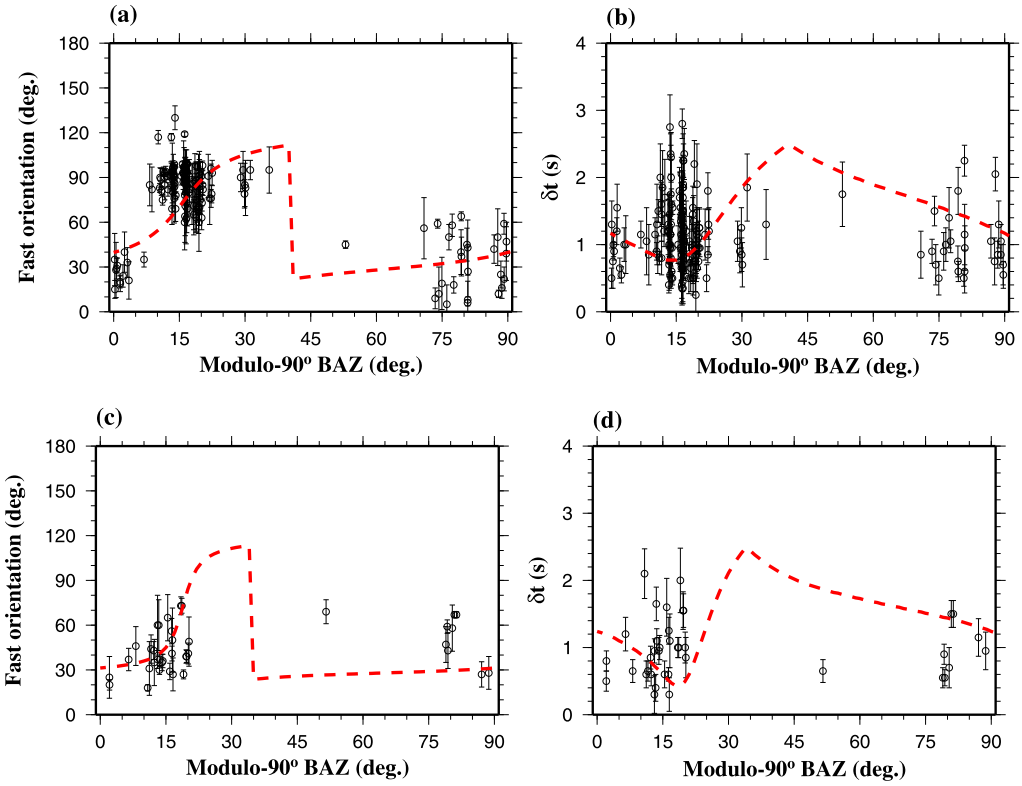

Fig. 7. Azimuthal variations of the fast orientations (left panels) and splitting times (right panels) for Group A (top panels) and Group B (bottom) measurements. In (a) and (b), the dashed lines are calculated values using the optimal splitting parameters obtained from grid-searching ($\phi_1 = 5°, \delta t_1 = 1.2$ s; $\phi_2 = 45°, \delta t_2 = 1.0$ s), and in (c) and (d), they represent theoretical values obtained using ($\phi_1 = 15°, \delta t_1 = 1.2$ s; $\phi_2 = 45°, \delta t_2 = 0.6$ s).

teristics of the SWS parameters across the profile (Fig. 2). If we assume that the termination of the Indian slab leads to significant changes in splitting parameters especially the splitting time, as previous studies suggested (Huang et al., 2000), the lack of a clear boundary in the spatial distribution of the observed splitting parameters indicates that the Indian slab does not terminate beneath the study area. This observation, when combined with the consistency between the fast orientation of the lower layer and the fast orientations observed in India (Fig. 1), favors the presence of the Indian slab beneath the study area, a conclusion that is consistent with previously suggested northern extent of the Indian slab (Fig. 1) beneath western Tibet (Kind and Yuan, 2010; Zhao et al., 2014b).

The absence of eastward asthenospheric flow beneath western Tibet could explain the paucity or rare presence of V-shaped conjugate strike-slip faults in this area. Such faults are abundant in central and eastern Tibet and were attributed to lithospheric basal shear by eastward flow in the asthenosphere and eastward escaping of the Tibetan lithosphere (Yin and Taylor, 2011).

Finally, the observations confirm the existence of plastic flow in the middle and/or lower crust beneath western Tibet. The existence of such flow is a debated issue (e.g., Tapponnier et al., 2001; Royden et al., 2008; Zhao et al., 2013; Zhang et al., 2014). The NE–SW oriented crustal anisotropy revealed by both the Pms and XKS phases provides additional support for the existence of such a flow, which is considered as the main cause for the uplift and growth of the Tibetan Plateau (Royden et al., 2008).

5. Conclusions

We have identified clear evidence of complex anisotropy beneath the Himalayan, Lhasa, and Qiangtang Blocks in western Tibet, along a N–S profile of about 400 km long. Grid-searching of individual layer parameters under a two-layer model with horizontal axes of symmetry indicates that the lower layer has a nearly N–S fast orientation, which is consistent with the fast orientations observed on the Indian continent, and can be explained by simple-shear induced anisotropy between the bottom of the lithosphere and the top of the asthenosphere. The upper layer has a NE–SW fast orientation, and the splitting parameters for the upper layer are comparable with those observed using P-to-S converted phases from the Moho, suggesting that the upper layer resides in the crust, probably related to plastic flow in the middle-lower crust. Additionally, this study demonstrates the importance of using the PKS and SKKS phases in addition to SKS for revealing the existence of complex anisotropy and characterizing realistic anisotropic structures.

Acknowledgements

We thank all the members in TPG-IGG, CAS who took part in the field work. We appreciate assistance and collaboration from Drs. Xiaobo Tian, Tao Xu, Zhiming Bai, Yun Chen, Xi Zhang, and Xiaofeng Liang. J. Wu is supported by National Natural Science Foundation of China under grants 41090291, 41090292, 41374064, 41074037. The study was partially supported by the U.S. National Science Foundation under award 0911346 to K. Liu and S. Gao.

References

Ammon, C.J., 1991. The isolation of receiver effects from teleseismic P waveforms. Bull. Seismol. Soc. Am. 81, 2504–2510.

Aspiroz, M.D., Lloyd, G.E., Fernandez, C., 2007. Development of lattice preferred orientation in clinoamphiboles deformed under low-pressure metamorphic conditions. A SEM/EBSD study of metabasites from the Aracena metamorphic belt (SW Spain). J. Struct. Geol. 29, 629–645.

Chen, W.P., Martin, M., Tseng, T., Nowack, R.L., Hung, S., Huang, B., 2010. Shear-wave birefringence and current configuration of converging lithosphere under Tibet. Earth Planet. Sci. Lett. 295, 297–304.

Chen, Y., Zhang, Z., Sun, C., Badal, J., 2013. Crustal anisotropy from Moho converted Ps wave splitting analysis and geodynamic implications beneath the eastern margin of Tibet and surrounding regions. Gondwana Res. 24, 946–957.
Crampin, S., 1981. A review of wave motion in anisotropic and cracked elastic-media. Wave Motion 3, 343–391.
Elsheikh, A.A., Gao, S.S., Liu, K.H., Mohamed, A.A., Yu, Y., Fat-Helbary, R.E., 2014. Seismic anisotropy and subduction-induced mantle fabrics beneath the Arabian and Nubian Plates adjacent to the Red Sea. Geophys. Res. Lett. 41, 2376–2381.
England, P., Molnar, P., 2005. Late quaternary to decadal velocity fields in Asia. J. Geophys. Res. 110, B12401. http://dx.doi.org/10.1029/2004JB003541.
Flesch, L.M., Holt, W.E., Silver, P.G., Stephenson, M., Wang, C.Y., Chan, W.W., 2005. Constraining the extent of crust-mantle coupling in central Asia using GPS, geologic, and shear wave splitting data. Earth Planet. Sci. Lett. 238, 248–268.
Gao, S.S., Liu, K.H., 2009. Significant seismic anisotropy beneath the southern Lhasa Terrane, Tibetan Plateau. Geochem. Geophys. Geosyst. 10, Q02008. http://dx.doi.org/10.1029/2008GC002227.
Huang, W.C., Ni, J.F., Tilmann, F., Nelson, D., Guo, J., Zhao, W., Mechie, J., Kind, R., Saul, J., Rapine, R., Hearn, T.M., 2000. Seismic polarization anisotropy beneath the central Tibetan Plateau. J. Geophys. Res. 105 (B12), 27 979–27 989.
Kent, C.C., 1989. Plate Tectonics and Crustal Evolution, third ed. Pergamon Press.
Kind, R., Yuan, X., 2010. Seismic images of the biggest crash on Earth. Science 329, 1479–1480.
Klemperer, L.S., 2006. Crustal flow in Tibet: geophysical evidence for the physical state of Tibetan lithosphere, and inferred patterns of active flow. In: Lae, R.D., Searle, M.P., Godin, L. (Eds.), Geol. Soc. (Lond.) Spec. Publ., 39–70. Special publications.
Kumar, P., Yuan, X., Kind, R., Kosarev, G., 2005. The lithosphere–asthenosphere boundary in the Tien Shan-Karakoram region from S receiver functions: evidence for continental subduction. Geophys. Res. Lett. 32, L07305. http://dx.doi.org/10.1029/2004GL022291.
Levin, V., Roecker, S., Graham, P., Hosseini, A., 2008. Seismic anisotropy indicators in Western Tibet: shear wave splitting and receiver function analysis. Tectonophysics 462, 99–108.
Li, C., van der Hilst, R.D., Meltzer, A.S., Engdahl, E.R., 2008. Subduction of the Indian lithosphere beneath the Tibetan Plateau and Burma. Earth Planet. Sci. Lett. 251, 293–304.
Liu, K.H., 2009. NA-SWS-1.1: a uniform database of teleseismic shear-wave splitting measurements for North America. Geochem. Geophys. Geosyst. 10, Q05011. http://dx.doi.org/10.1029/2009GC002440.
Liu, K.H., Gao, S.S., 2013. Making reliable shear-wave splitting measurements. Bull. Seismol. Soc. Am. 103, 2680–2693. http://dx.doi.org/10.1785/0120120355.
Liu, H., Niu, F., 2012. Estimating crustal seismic anisotropy with a joint analysis of radial and transverse receiver function data. Geophys. J. Int. 188, 144–164.
Liu, K.H., Gao, S.S., Gao, Y., Wu, J., 2008. Shear wave splitting and mantle flow associated with the deflected slab beneath northeast Asia. J. Geophys. Res. 113, B01305. http://dx.doi.org/10.1029/2007JB005178.
Liu, Q.Y., van der Hilst, R.D., Li, Y., Yao, H.J., Chen, J.H., Guo, B., Qi, S.H., Wang, J., Huang, H., Li, S.C., 2014. Eastward expansion of the Tibetan Plateau by crustal flow and strain partitioning across faults. Nat. Geosci. 7, 361–365. http://dx.doi.org/10.1038/NEGO2130.
McNamara, D.E., Owens, T.J., 1993. Azimuthal shear wave velocity anisotropy in the basin and range province using Moho Ps converted phases. J. Geophys. Res. 98 (B7), 12 003–12 017.
McNamara, D.E., Owens, T.J., Silver, P.G., Wu, F.T., 1994. Shear wave anisotropy beneath the Tibetan Plateau. J. Geophys. Res. 99, 13 655–13 665.
Molnar, P., Tapponnier, P., 1975. Cenozoic tectonics of Asia: effects of a continental collision. Science 189, 419–426.
Molnar, P., England, P., Martinod, J., 1993. Mantle dynamics, uplift of the Tibetan plateau, and the Indian monsoon. Rev. Geophys. 31, 357–396.
Nelson, K.D., Zhao, W., Brown, L.D., Kuo, J., Che, J., Liu, X., Klemperer, S.L., Makovsky, Y., Meissner, R., Mechie, J., Kind, R., Wenzel, F., Ni, J., Nabelek, J., Leshou, C., Tan, H., Wei, W., Jones, A.G., Booker, J., Unsworth, M., Kidd, W.S.F., Hauck, M., Alsdorf, D., Ross, A., Cogan, M., Wu, C., Sandvol, E., Edwards, M., 1996. Partially molten middle crust beneath southern Tibet: synthesis of project INDEPTH results. Science 274, 1684–1688.
Okaya, D., Christensen, N., Stanley, D., Stern, T., 1995. Crustal anisotropy in the vicinity of the Alpine Fault Zone. N.Z. J. Geol. Geophys. 38, 579–583.
Oreshin, S., Kiselev, S., Vinnik, L., Prakasam, K.S., Rai, S.S., Makeyeva, L., Savvin, Y., 2008. Crust and mantle beneath western Himalaya, Ladakh and western Tibet from integrated seismic data. Earth Planet. Sci. Lett. 271, 75–87.
Ozacar, A.A., Zandt, G., 2004. Crustal seismic anisotropy in central Tibet: implications for deformational style and flow in the crust. Geophys. Res. Lett. 31, L23601. http://dx.doi.org/10.1029/2004GL021096.
Royden, L.H., Burchfiel, B.C., van der Hilst, R.D., 2008. The geological evolution of the Tibetan Plateau. Science 321, 1054–1058.
Rumpker, G., Kaviani, A., Latifi, K., 2014. Ps-splitting analysis for multilayered anisotropic media by azimuthal stacking and layer stripping. Geophys. J. Int. 199, 146–163.
Sandvol, E., Ni, J., Kind, R., Zhao, W., 1997. Seismic anisotropy beneath the southern Himalaya–Tibet collision zone. J. Geophys. Res. 102, 17 813–17 823.
Savage, M.K., 1999. Seismic anisotropy and mantle deformation: what have we learned from shear wave splitting? Rev. Geophys. 37, 65–106.
Silver, P.G., 1996. Seismic anisotropy beneath the continents: probing the depths of geology. Annu. Rev. Earth Planet. Sci. 24, 385–432.
Silver, P.G., Chan, W.W., 1991. Shear wave splitting and subcontinental mantle deformation. J. Geophys. Res. 96, 16,429–16,454.
Silver, P.G., Savage, M., 1994. The interpretation of shear-wave splitting parameters in the presence of two anisotropic layers. Geophys. J. Int. 119, 949–963.
Tapponnier, P., Xu, Z., Roger, F., Meyer, B., Arnaud, N., Wittlinger, G., Yang, J., 2001. Oblique stepwise rise and growth of the Tibet Plateau. Science 294, 1671–1677.
Tatham, D.J., Lloyd, G.E., Butler, R.W.H., Casey, M., 2008. Amphibole and lower crustal seismic properties. Earth Planet. Sci. Lett. 267, 118–128.
Taylor, M., Yin, A., 2009. Active structures of the Himalayan–Tibetan orogen and their relationships to earthquake distribution, contemporary strain field, and Cenozoic volcanism. Geosphere 5 (3), 199–214. http://dx.doi.org/10.1130/GES00217.1.
Tilmann, F., Ni, J., INDEPTH III Seismic Team, 2003. Seismic imaging of the downwelling Indian lithosphere beneath central Tibet. Science 300, 1424–1427.
Yeck, W.L., Sheehan, A.F., Schulte-Pelkum, V., 2013. Sequential H–K stacking to obtain accurate crustal thicknesses beneath sedimentary basins. Bull. Seismol. Soc. Am. 103, 2142–2150. http://dx.doi.org/10.1785/0120120290.
Yin, A., Harrison, T.M., 2000. Geologic evolution of the Himalayan–Tibetan orogen. Annu. Rev. Earth Planet. Sci. 28, 211–280.
Zhang, S., Karato, S., 1995. Lattice preferred orientation of olivine aggregates deformed in simple shear. Nature 375, 774–777.
Yin, A., Taylor, M.H., 2011. Mechanics of V-shaped conjugate strike-slip faults and the corresponding continuum mode of continental deformation. Geol. Soc. Bull. 123, 1798–1821.
Zhang, Z., Wang, Y., Houseman, G., Xu, T., Wu, Z., Yuan, X., Chen, Y., Tian, X., Bai, Z., Teng, J., 2014. The Moho beneath western Tibet: shear zones and eclogitization in the lower crust. Earth Planet. Sci. Lett. 408, 370–377.
Zhao, W.L., Morgan, W.J., 1987. Injection of Indian crust into Tibetan lower crust. Tectonics 6, 489–504. http://dx.doi.org/10.1029/TC006i004p00489.
Zhao, J., Yuan, X., Liu, H., Kumar, P., Pei, S., Kind, R., Zhang, Z., Teng, J., Ding, L., Gao, X., Xu, Q., Wang, W., 2010. The boundary between the Indian and Asian tectonic plates below Tibet. Proc. Natl. Acad. Sci. USA 107 (25), 11 229–11 233.
Zhao, L., Xie, X., He, J., Tian, X., Yao, Z., 2013. Crustal flow pattern beneath the Tibetan Plateau constrained by regional Lg-wave Q tomography. Earth Planet. Sci. Lett. 383, 113–122.
Zhao, J., Murodov, D., Huang, Y., Sun, Y., Pei, S., Liu, H., Zhang, H., Fu, Y., Wang, W., Cheng, H., Tant, W., 2014a. Upper mantle deformation beneath central–southern Tibet revealed by shear wave splitting measurements. Tectonophysics 627, 135–140.
Zhao, J., Zhao, D., Zhang, H., Liu, H., Huang, Y., Cheng, H., Wang, W., 2014b. P-wave tomography and dynamics of the crust and upper mantle beneath western Tibet. Gondwana Res. 25, 1690–1699. http://dx.doi.org/10.1016/j.gr.2013.06.020.
Zheng, H., Li, T., Gao, R., Zhao, D., He, R., 2007. Teleseismic P-wave tomography evidence for the Indian lithospheric mantle subducting northward beneath the Qiangtang terrane. Chin. J. Geophys. 50, 1418–1426.
Zhou, H., Murphy, M.A., 2005. Tomographic evidence for wholesale underthrusting of India beneath the entire Tibetan plateau. J. Asian Earth Sci. 25, 445–457.